Solar Energy 231 (2022) 1–7

Contents lists available at ScienceDirect

Solar Energy

journal homepage: www.elsevier.com/locate/solener

Solution-processed vanadium oxides as a hole-transport layer for Sb_2Se_3 thin-film solar cells

Al Amin [a,1], Liping Guo [a,1], S.N. Vijayaraghavan [a], Dian Li [b], Xiaomeng Duan [a], Harigovind G. Menon [a], Jacob Wall [a], Subhadra Gupta [a], Mark Ming-Cheng Cheng [c], Yufeng Zheng [b], Lin Li [a], Feng Yan [a,*]

[a] Department of Metallurgical and Materials Engineering, The University of Alabama, Tuscaloosa, AL 35487, USA
[b] Department of Chemical and Materials Engineering, University of Nevada Reno, 1664 N. Virginia St., Reno, NV 89557 USA
[c] Department of Electrical and Computer Engineering, The University of Alabama, Tuscaloosa, AL 35487, USA

A R T I C L E I N F O

Keywords:
Sb_2Se_3
Thin-film solar cells
VO_x
Hole-transport layer
Open-circuit voltage

A B S T R A C T

Antimony selenide (Sb_2Se_3) is a promising light absorber material for solar cells because of its superior photovoltaic properties. However, the current performance of the Sb_2Se_3 solar cell is much lower than its theoretical value (~32%) due to its low open-circuit voltage (V_{OC}). In this paper, we have demonstrated inorganic vanadium oxides (VO_x) as a hole transport layer (HTL) for Sb_2Se_3 solar cells to enhance efficiency through the V_{OC} improvement. Here, a solution-processed VO_x through the decomposition of the triisopropoxyvanadium (V) oxide is deposited on the Sb_2Se_3 absorber layer prepared by close-spaced sublimation (CSS). With VO_x HTL, the built-in voltage (V_{bi}) is significantly increased, leading to improved V_{OC} for the Sb_2Se_3 solar cell devices. As a result, the efficiency of the device increases from an average efficiency of 5.5% to 6.3% with the VO_x.

1. Introduction

Solar cell technology is one of the most promising approaches to directly convert solar energy into electricity, and thus protect our environment from the greenhouse effect and reduce the carbon footprint (Crabtree and Lewis, 2007; El Chaar et al., 2011; Nayak et al., 2019). In general, thin film solar cell technology based on cadmium telluride (CdTe) and copper indium gallium selenide (CIGS) has achieved a power conversion efficiency (*PCE*) of 22.1% and 23.35%, respectively (Green et al., 2020; Green et al., 2018). However, the toxicity of Cd and the high cost of Ga and In are driving people to look for low-cost, environmentally friendly, and abundant materials for the development of a sustainable solar energy economy (Zakutayev, 2017). Recently, antimony chalcogenide, e.g., Sb_2Se_3 has drawn more attention due to its environmentally benign, low-cost, excellent light absorption coefficient ($>10^5$ cm^{-1} for the sunlight), and desirable bandgap (1.1–1.2 eV) (Mavlonov et al., 2020; Zeng et al., 2016). Moreover, Sb_2Se_3 exhibits a ribbon-like quasi-one-dimensional (Q1D) crystalline structure with self-passivated grains boundaries, which prevents the traditional cubic absorbers carrier recombination in the grain boundaries (Guo et al., 2018a; Li et al., 2019; Wang et al., 2017; Zeng et al., 2016; Zhou et al., 2015).

The power conversion efficiency (PCE) of Sb_2Se_3 solar cells has been greatly improved from 5% to 9.2% in the past five years. This repaid PCE growth benefits from the improved absorber growth techniques (e.g., vapor transport deposition, close space sublimation, and hydrothermal), buffer layer optimization (e.g., ZnO, CdTe, and TiO_2), and new device architecture design. (Lei et al., 2019; Mavlonov et al., 2020; Wang et al., 2017) However, the low photovoltage of the Sb_2Se_3 solar cells significantly limits the device's performance improvement. The theoretical calculation indicates that negative band bending should be suppressed to extract more holes to the back contact (Leng et al., 2014; Li et al., 2020; Shen et al., 2020). Thus, the hole transport layer (HTL) becomes more important in the antimony chalcogenides solar cells. For example, the efficiency of Sb_2Se_3 cell was improved from 5.42% to 6.50% by using inorganic PbS colloidal quantum dot film as HTL (Chen et al., 2017). Inorganic CuSCN HTL was introduced to Sb_2Se_3 solar cells and boost the device efficiency up to 7.5% (Li et al., 2019). Especially, 2,2,7,7-tetrakis (N,N-di-p-methoxyphenylamine)-9,9-spirobi-fluorene (Spiro-OMeTAD) is the most used HTL and also was used for the $Sb_2(S, Se)_3$ solar cells and demonstrated PCE ~ 10%.(Jiang et al., 2021; Wang et al., 2019)

* Corresponding authors.
E-mail address: fyan@eng.ua.edu (F. Yan).
[1] Equal contribution.

https://doi.org/10.1016/j.solener.2021.11.009
Received 24 August 2021; Received in revised form 23 October 2021; Accepted 5 November 2021
Available online 23 November 2021

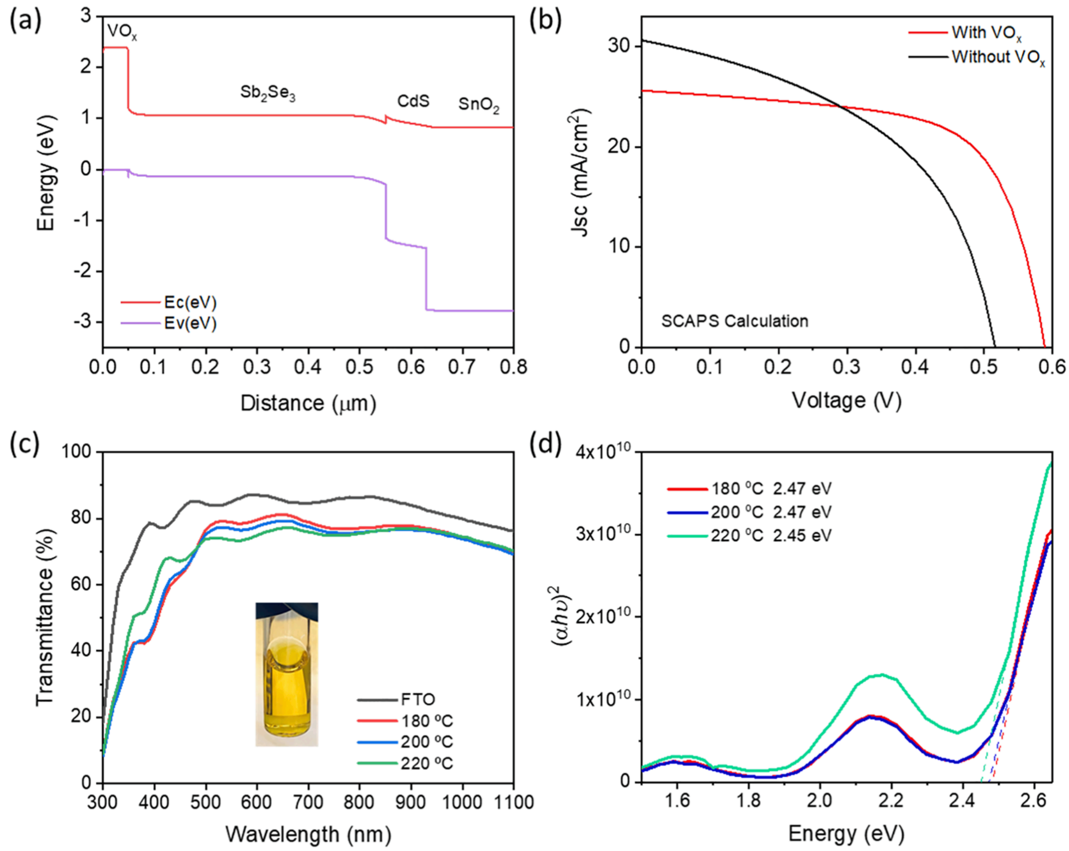

Fig. 1. (a) Energy band structure, and (b) current–voltage (J-V) curve of the FTO/CdS/Sb_2Se_3/VO_x/Au device obtained from SCAPS simulation. (c) Optical transmittance (the inset shows the VTIPO solution), and (d) corresponding energy bandgap of the VO_x films annealed at various temperatures.

However, the organic HTLs face instability issues in the device performance, and the high cost also limits their upscale manufacturing. Therefore, it is necessary to develop cost-effective, non-toxic, stable material to use at the interface to obtain high-efficiency PV cells.

As for the inorganic HTL materials, vanadium oxides, i.e., VO_x was widely used for the organic and perovskite solar cells(Chu et al., 2018), and have been successfully applied to the Sb_2S_3 solar cells with improved PCE. (Zhang et al., 2018) Particularly, the reported conduction band (CB) and valence band (VB) of VO_x are 2.94 eV and 5.36 eV, (Chen et al., 2011; Peng et al., 2016b) which align well with Sb_2Se_3 solar cells with CB ~ 4.15 eV and VB 5.35 eV, respectively.(Das et al., 2020) So far, there is a limited report for the VO_x as HTL for the Sb_2Se_3 solar cells. In this work, we combine the device simulation and experimental validation of the solution-processed VO_x HTL for the Sb_2Se_3, and successfully demonstrated an improved device performance with VOx as HTLs for a high-efficiency Sb_2Se_3 solar cell.

2. Experimental methods

2.1. SCAPS device simulation

The device simulation with the VO_x HTL for the n-i-p device was performed using the solar cell capacitance simulator (SCAPS) with an F-doped-SnO_2/CdS/Sb_2Se_3/VO_x/Au architecture. The parameters of materials for SCAPS simulations were obtained from the previously reported materials parameters and defects values (Ahmmed et al., 2021; Chen et al., 2017).

2.2. Sb_2Se_3 film deposition

Commercial fluorine-doped SnO_2 (FTO) coated soda-lime glass (TEC 10, NSG, US) was cleaned with detergent, acetone, isopropanol, and deionized water in sequence in the ultrasonic bath. CdS window layer was deposited on the cleaned FTO glass via a chemical bath deposition. (Guo et al., 2018b) The Sb_2Se_3 absorber layer with 0.5 μm-thickness was grown in a close-spaced sublimation (CSS) system under vacuum with deposition pressure of ~ 10 mTorr, where the top and bottom heaters were controlled at 300 and 550 °C during deposition, respectively.

2.3. Vo_x hole-transport layer fabrication and device fabrication

The V_2O_5 precursor solution was prepared according to the literature reported previously (Zhang et al., 2018). In brief, 0.25 mL vanadium(V) tri-isopropoxide oxide (VTIPO, 97%, Tokyo Chemical Industry Co., LTD) was dissolved into 3.8 mL isopropanol (IPA) and 0.2 mL deionized water (DIW) mixture, then stirred vigorously for 30 min until the color turned to light yellow. VTIPO solution was spin-coated on the Sb_2Se_3 films at 3000 rpm for 30 s, followed by annealing on a hotplate at various temperatures (120 °C to 220 °C) for 10 min in a dry N_2 filled glovebox to form the VO_x hole transport layer. The device with architecture FTO/CdS/Sb_2Se_3/V_2O_5/Au was completed by sputtering the Au electrode using the sputtering system (AJA ATC Orient 5) with a 2-inch Au target, with the cell area defined as 0.09 cm^2 by a shadow mask.

2.4. Materials characterization

The thickness of the Sb_2Se_3 films was characterized by the SEM cross-section image. The film morphology and chemical composition were characterized by the scanning electron microscope (SEM, JEOL 7000) and energy-dispersive spectroscopy (EDS) attached to the SEM. The transmittance spectra were characterized by a UV–Vis measurement system. The surface roughness was measured in a Park System atomic

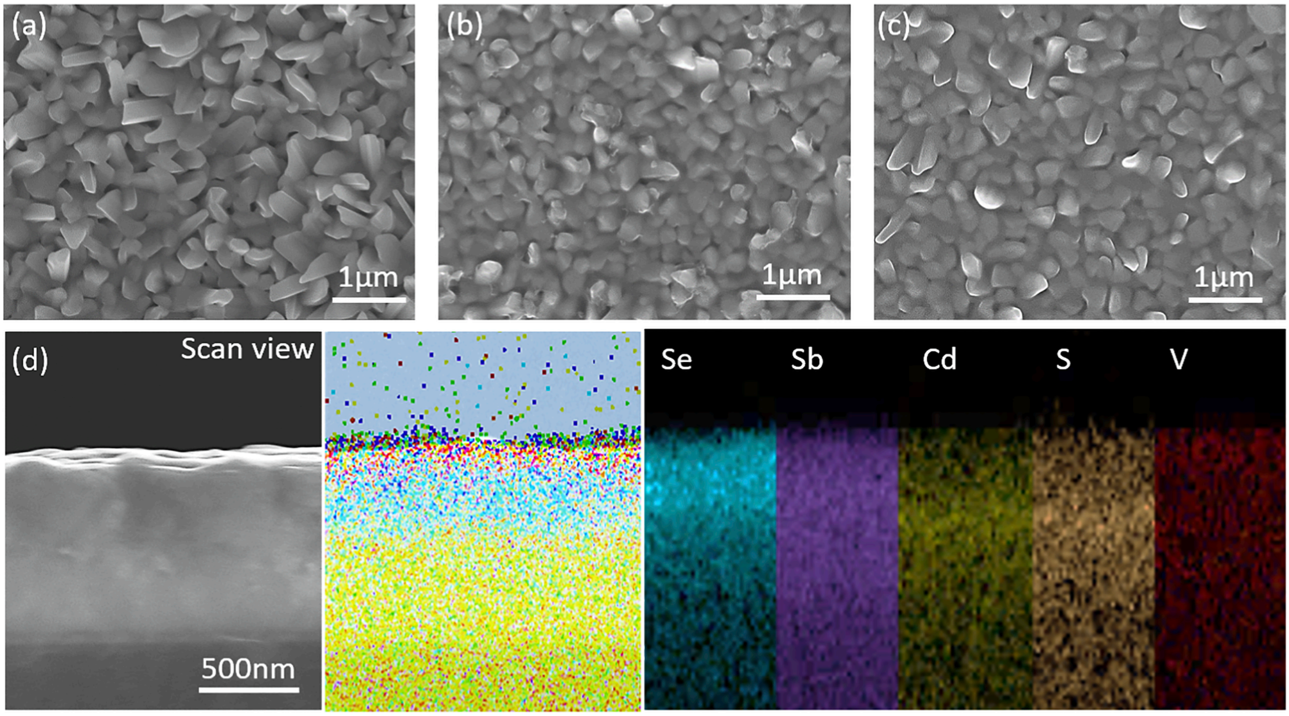

Fig. 2. SEM morphology for (a) bare Sb_2Se_3 film, (b) VOx coated Sb_2Se_3 with 100 °C annealing for 10 min, (c) VO_x coated Sb_2Se_3 film with 200 °C annealing for 10 min. (d) Cross-sectional SEM of the VO_x coated Sb_2Se_3 with the corresponding EDS elemental mapping images of constituent elements.

force microscopy (AFM). The contact angle was obtained in a contact angle meter. The capacitance–voltage (CV) measurements were performed in a Keithley 4200 semiconductor parameter analyzer (Tektronix 4200A-SCS, USA) at room temperature in darkness at a frequency of 1 kHz and AC amplitude of 30 mV

2.5. Solar cell measurement

The current density–voltage (*J-V*) curve of the fabricated solar cells was characterized using a solar simulator (Newport, Oriel Class AAA 94063A, 1000 Watt Xenon light source) with a source meter (Keithley 2420) at 100 mW cm^{-2} AM 1.5 G irradiation. A calibrated Si-reference cell and meter (Newport, 91150 V, certified by NREL) was used to calibrate the solar simulator prior to the measurement. External Quantum Efficiency (EQE) of solar cells was obtained by the solar cell spectra response measurement system (QE-T, Enli Technology, Co. Ltd). Capacitance-Voltage (*C-V*) measurement was performed in the dark at room temperature using a Keithley 4200 semiconductor parameter analyzer (Tektronix 4200A-SCS, USA).

3. Results and discussion

To confirm if the VO_x was a suitable hole transport layer for the Sb_2Se_3 solar cells, we simulated SCAPS devices before the experiment. As shown in Fig. 1a, the VO_x layer has a suitable band position to match the valence band of Sb_2Se_3 to promote the photogenerated hole extraction, while the conduction band can block the photoexcited electron and prevent electron-hole recombination at the back surface. Therefore, in principle, the VO_x should play as both the hole transport and electron block layer. Promisingly, the SCAPS current density–voltage simulation (J-V) as shown in Fig. 1b, suggests that the Sb_2Se_3 without VO_x HTLs possess a lower power conversion efficiency (PCE ~ 7.5% with V_{OC} = 0.517 V, J_{SC} ~ 30.6 $mAcm^{-2}$, FF ~ 47.8%) By the introduction of the thin VO_x HTL (~50 nm), the device performance is improved to 10.2% with V_{OC} = 0.591 V, J_{SC} ~ 26.7 $mAcm^{-2}$, FF ~ 64.6%, benefiting from the improved charge collection and reduced carrier recombination at the back surface. Therefore, we systematically explore the device performance of the VO_x HTL on the Sb_2Se_3 solar cells by tailoring the VO_x synthesized annealing condition.

The as-prepared solution exhibited a light yellow color, as indicated in the inset of Fig. 1(c). The light transmittance of the VO_x films spin-coated on the FTO glass substrate and annealed under various temperatures was characterized (Fig. 1b). The V_2O_5 films (~50 nm) show a transmittance lower than that of the FTO substrate, suggesting that the VO_x films can absorb certain sunlight, particularly, for the short-wavelength light. With increasing the annealing temperature, the overall transmittance was not significantly changed, indicating a stable VO_x layer was formed. The bandgap for the VO_x films determined by the Tauc plots derived from the transmittance is shown in Fig. 1(d). The VO_x films annealed at different temperatures exhibited a similar bandgap of ~ 2.45 to 2.47 eV. It was reported that the oxidation states of V in VO_x, e.g., V^{4+} and V^{5+} would be impacted by the annealing temperature, and V^{4+} contributed to the improved conductivity of VO_x gradually increased with increasing the annealing temperature (Manno et al., 1997; Peng et al., 2016a; Zhang et al., 2018; Zilberberg et al., 2011). This bandgap of VO_x was slightly narrower than that of the V_2O_5 film with 2.65 eV reported, suggesting a higher annealing temperature preferred the formation of VO_x and could promise better charge extraction and valence match between VO_x and Sb_2Se_3.

The surface morphology of the VO_x on the Sb_2Se_3 thin film solar cell was characterized using scanning electron microscopy (SEM). As shown in Fig. 2(a)-(c), the as-deposited Sb_2Se_3 film exhibits a rough surface with rod structures that were associated with the orthorhombic crystal structure of Sb_2Se_3 and the fast deposition rate of the CSS, and in agreement with the previous report.(Guo et al., 2018a; Guo et al., 2019) In general, the rough surfaces of the Sb_2Se_3 film are not desired for solar cell devices, as the back contact/electrode might not be able to form a complete contact with the Sb_2Se_3 due to the existence of the voids and protrusions, which hinders the charge carrier transfer in this region. With the VO_x HTL coated on the Sb_2Se_3 annealed at 100 °C, the voids are filled with the VO_x, while the film becomes dense and smooth. By increasing the annealing temperature to 200 °C, the VO_x coated Sb_2Se_3

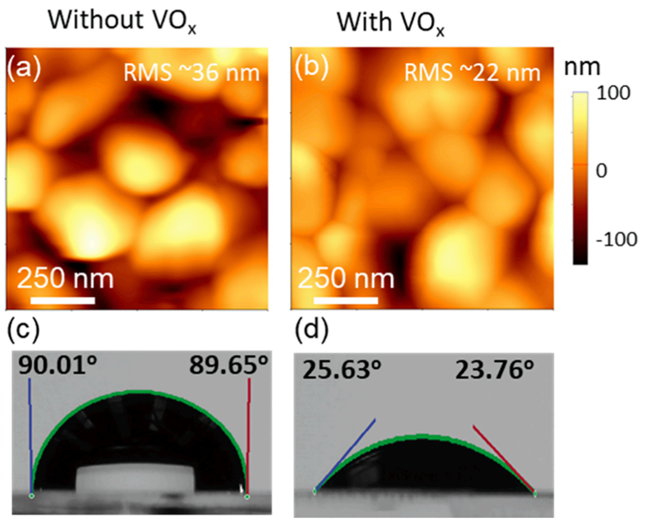

Fig. 3. Atomic force microscopy surface morphology of the Sb_2Se_3 without (a) and with (b) VO_x HTLs. Water contact angle on the (c) bare Sb_2Se_3 surface and (d) VOx surface.

surface becomes more denser and smoother. On some portions of the VO_x coated Sb_2Se_3 surface show the sharp nanorod round. This could be due to the decomposition of VO_x precursor (VTIPO) on the Sb_2Se_3 surface during heating of an exothermic reaction. (Prześniak-Welenc et al., 2015). Fig. 2d shows the cross-sectional image of VO_x coated Sb_2Se_3 characterized using X-ray energy dispersive spectroscopy (EDS). The elements mapping demonstrates that the Sb_2Se_3 is pretty uniform and the VO_x were limited diffused into the bulk of the Sb_2Se_3 layer.

Fig. 3a and 3b show the atomic force microscopy (AFM) surface morphology of the bare and the VO_x coated Sb_2Se_3, respectively. The root-mean-square (RMS) roughness value of the bare Sb_2Se_3 was 36 nm, while the VO_x coated Sb_2Se_3 become smooth and the RMS ~ 22 nm, which was in line with the SEM observation. Here, the surface energy of the VO_x layer was evaluated using the contact angle measurements as shown in Fig. 3c-d. The bare Sb_2Se_3 show a contact angle ~ 90°, suggesting poor wetting. With the VO_x HTL applied, the contact angle significantly reduces to ~ 25° and surfaces becomes hydrophilic which are similar result measured by T. Chang el al. (Chang et al., 2019). The reduction in contact angle after depositing VO_x thin layer on Sb_2Se_3 can be attributed to the reduced surface roughness and the intrinsic hydrophilicity of VOx (Fang et al., 2020; Yang et al., 2006). However, this hydrophilic VO_x HTL suggests that the VO_x HTL may be suitable as a buffer layer for the back contact using the printing techniques, such as doctor-blade carbon paste or metal inks.

To investigate the effect of the VO_x HTL on the Sb_2Se_3 solar cells, we fabricated devices in the configuration of FTO/CdS/Sb_2Se_3/VO_x/Au, as shown in Fig. 4(a). Au electrodes were sputtered on the VO_x coated Sb_2Se_3 films with a thickness of ~80 nm. The energy band diagram of the device is plotted in Fig. 4(b), where the VBM and CBM of the VO_x layer were reported elsewhere. (Chen et al., 2011). As predicated using SCAPS, the band alignment between the Sb_2Se_3 and VO_x could promote the carrier collection. The experimental J-V curves were measured under 1 sun (AM 1.5G) illumination, as shown in Fig. 4c. The device without VO_x HTL has a lower device performance with PCE ~ 5.5% due to the low V_{OC} ~ 0.358 V and fill factor (FF) ~ 48.5%. The device based

Table 1
Champion Device parameters of Sb_2Se_3 solar cells with and without VO_x HTL.

Samples	V_{OC}, V	*Jsc*, mA/cm^2	*FF*, %	*PCE*, %
Without VO_x	0.358	31.89	48.52	5.53
With VO_x	0.409	31.62	48.96	6.33

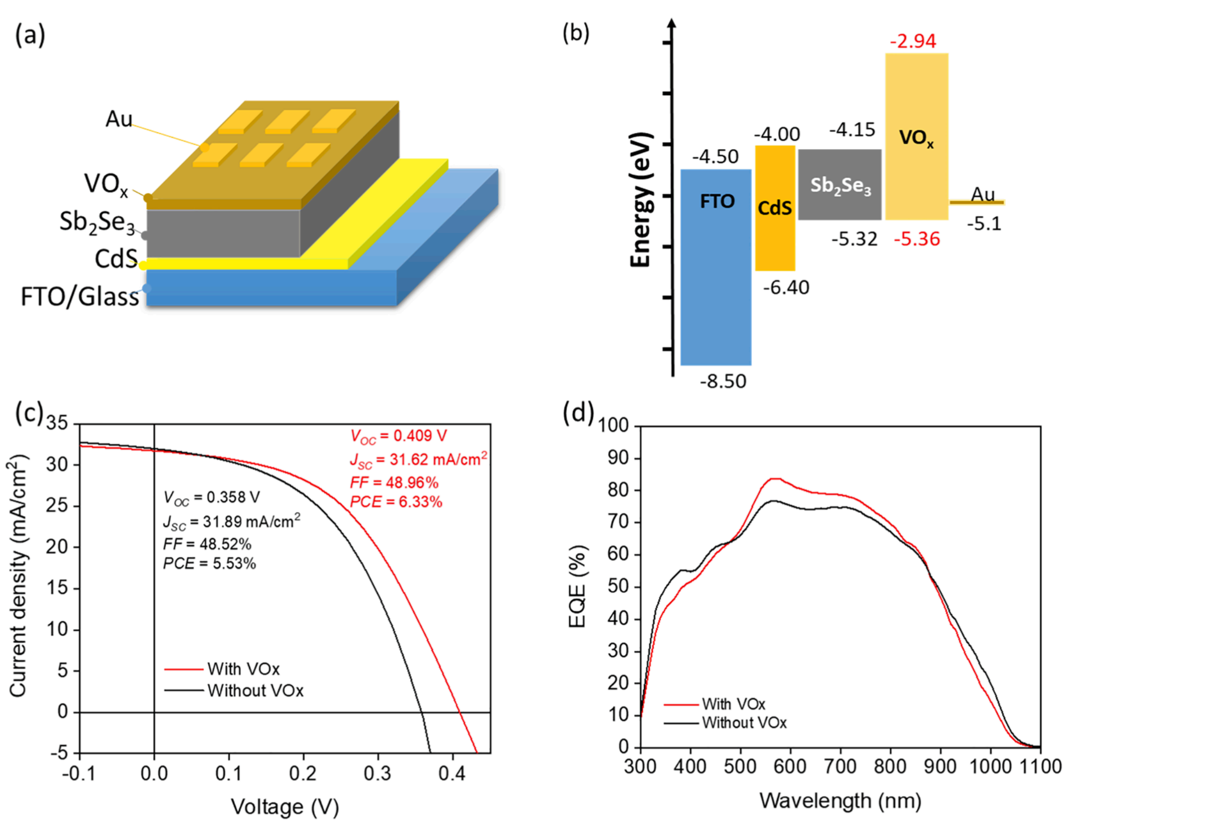

Fig. 4. (a) Schematic illustration of Sb_2Se_3 device configuration. (b) Schematic of the energy band diagram of the Sb_2Se_3 cells with VO_x hole transport layer. (c) *J-V* curves and (d) *EQE* spectra of the champion Sb_2Se_3 cells with and without the VO_x layer.

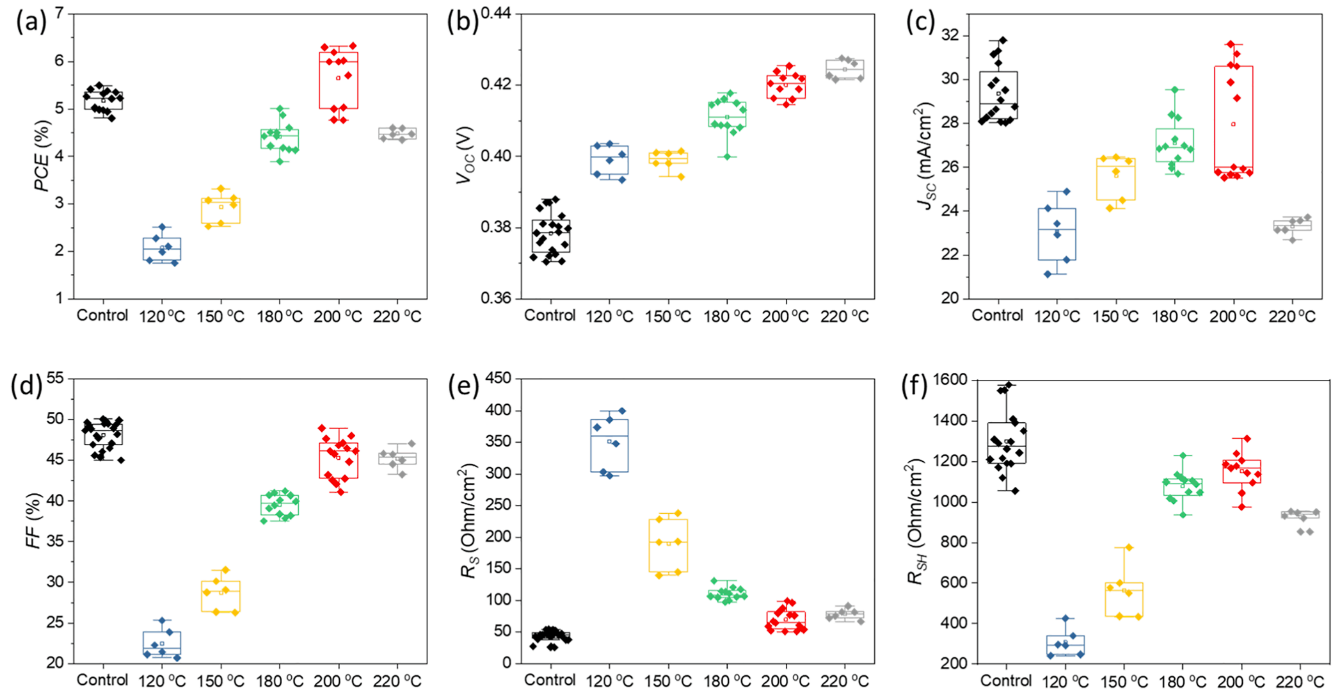

Fig. 5. Statistical distributions of (a) *PCE*, (b) V_{OC}, (c) J_{SC}, (d) *FF*, (e) R_S, and (f) R_{SH} of Sb_2Se_3 solar cells with VO_x as the HTL with various annealing temperatures from 120 to 220 °C.

on the VO_x HTL has a dramatically improved V_{OC} ~ 0.409 V and PCE of ~ 6.33%, while the current and FF with limited change. The detailed device performance is listed in Table 1. Note that the control device has a relatively low V_{OC}, which could be attributed to the thin Sb_2Se_3 absorber layer, which is ~ 500 nm (Fig. 2d). Traditionally, for the physical vapor deposited Sb_2Se_3 devices, such as rapid thermal evaporation (RTE), CSS, and VTD to achieve a decent V_{OC} above 0.4 V, (Guo et al., 2018a; Wen et al., 2018; Zhou et al., 2015) the thickness of the absorber layer normally need ~ 1 μm.(Li et al., 2018; Li, Zhiqiang et al., 2019; Wen et al., 2018) Here, with the VO_x HTL, it is successfully demonstrated that the physical vapor deposited Sb_2Se_3 thin film with a thickness of 500 nm can also achieve a high V_{OC} by suppressing the photogenerated carrier recombination at the back surface. This also demonstrates that the VO_x HTL can be used to replace the organic HTL, such as the Spiro-OMeTAD, PTAA, and P3HT.

To better understand the performance improvement, external quantum efficiency (EQE) was carried out (Fig. 3d). Here we chose the VO_x annealed at the 200 °C with the best device performance (discuss later) as a model system for the EQE measurement. The device with VO_x shows a better light response in the medium wavelength region of ~ 500 to 850 nm than that without VO_x. In the short-wavelength (<500 nm), the device without VO_x collects more photogenerated electrons, suggesting that the heating may also induce the CdS/Sb_2Se_3 interdiffusion and leads to a buried junction in the front end.(Zhou et al., 2017) In the long-wavelength (>850 nm), the carrier collection in the VO_x-based devices becomes weak, suggesting that the photogenerated electron may be reflected at the back surface and recombined with the photogenerated holes due to the higher conduction band of VO_x than that of the Sb_2Se_3.

To investigate the optimial annealing temperature of the VO_x coating layer, the as-deposited VO_x layer was annealed at various temperatures ranging from 120 to 220 °C in the N_2 filled glovebox for 10 min. The statistical distribution of the device parameters with different annealing temperatures is shown in Fig. 5. The device performance increases with increasing annealing temperature from 120 up to 200 °C, with an average *PCE* from ~ 2% to ~ 6%. The initially low performance majorly comes from the high series resistivity (R_S), which could be associated with the incomplete decomposition of the VTIPO. With increasing the

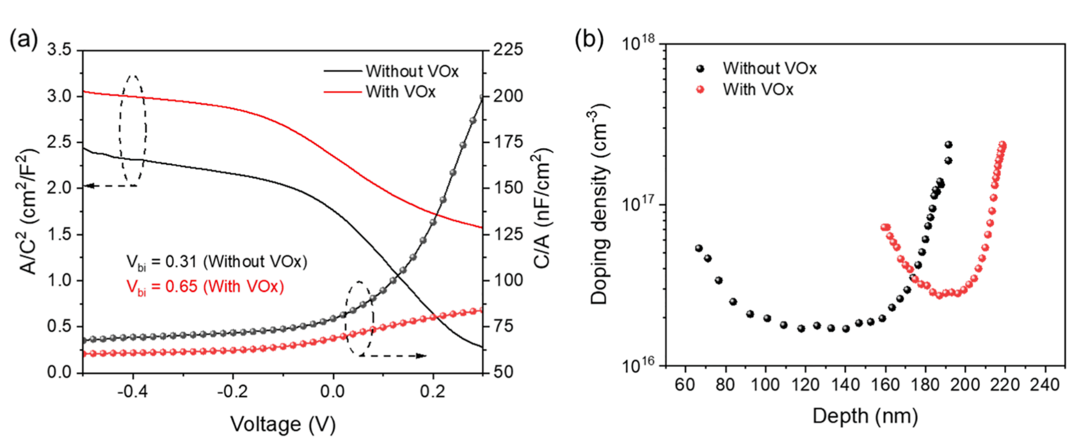

Fig. 6. (a) A/C^2 and C/A versus applied voltage (V) graphs. (b) Logarithmic representation of a C-V derived carrier density profiles.

temperature, the VTIPO decomposes,(Zhang et al., 2018) and the VO_x layer formed and contribute the significantly reduced Rs and improved *V*oc, Jsc, and FF. When the temperature further increases from 200 to 220 °C, the device performance drops from the peak PCE of 6% to ~ 4.5%. The potential reason is that the higher anneal temperature may change the valence band and impact the hole collection.

To determine the origin of the improved *V*oc with the VO_x, capacitance–voltage (C-V) measurement was conducted to reveal its built-in voltage V_{bi} and doping density. Fig. 6a shows the Mott-Schottky plot of the Sb_2Se_3 solar cell devices with and without VO_x. With the VO_x HTL, the V_{bi} of the solar cell increased from 0.31 V to 0.65 V, which demonstrated that the increased V_{OC} theoretically originated from the improved V_{bi}., which benefits from the band bending at the Sb_2Se_3/VO_x interface. The carrier concentration in the bare Sb_2Se_3 and the Sb_2Se_3 with VO_x was characterized through the CV profiling, as shown in Fig. 6b. The doping density of the device with the VO_x is $\sim 3 \times 10^{16}$ cm^{-3} while the control device is $\sim 2 \times 10^{16}$ cm^{-3}, indicating the VO_x could improve the carrier concentration and prevent the carrier recombination at the backside, suggesting the interfacial defect density was reduced in the Sb_2Se_3 absorbers.

4. Conclusions

In summary, we successfully demonstrated VO_x as an effective HTL for Sb_2Se_3 thin-film solar cells. After optimizing the annealing temperature of VO_x, the device performance of Sb_2Se_3 solar cells was significantly improved from an average *PCE* of ~ 5% to ~ 6%. dominating by the significantly improved V_{OC} from an average of ~ 0.35 V to 0.41 V. The improved V_{OC} is associated with the increased build-in voltage and the carrier concentration. Particularly, the VO_x formation temperature is critical for the device performance and it was demonstrated that 200 °C is desired to form the hole transport and electron blocking layer. This work provides an effective hole-transporting material for Sb_2Se_3 solar cells, which could significantly address the V_{OC} deficit at a low cost.

Declaration of Competing Interest

The authors declare that they have no known competing financial interests or personal relationships that could have appeared to influence the work reported in this paper.

Acknowledgments

This work is supported by National Science Foundation under contracts No. 1944374, 2019473 and 2127640, National Aeronautics and Space Administration, Alabama EPSCoR International Space Station Flight Opportunity program (contract# 80NSSC20M0141), and USDA National Institute of Food and Agriculture, AFRI project award (contract# 2020-67022-31376). D. Li and Y. Zheng appreciate the financial support by the faculty startup funding from University of Nevada Reno.

References

Ahmmed, S., Aktar, A., Ismail, A.B.M., 2021. Role of a Solution-Processed V2O5 Hole Extracting Layer on the Performance of CuO-ZnO-Based Solar Cells. ACS Omega 6 (19), 12631–12639.

Chang, T., Cao, X., Li, N., Long, S., Zhu, Y., Huang, J., Luo, H., Jin, P., 2019. Mitigating Deterioration of Vanadium Dioxide Thermochromic Films by Interfacial Encapsulation. Matter 1 (3), 734–744.

Chen, C.-P., Chen, Y.-D., Chuang, S.-C., 2011. High-Performance and Highly Durable Inverted Organic Photovoltaics Embedding Solution-Processable Vanadium Oxides as an Interfacial Hole-Transporting Layer. Adv. Mater. 23 (33), 3859–3863.

Chen, C., Wang, L., Gao, L., Nam, D., Li, D., Li, K., Zhao, Y., Ge, C., Cheong, H., Liu, H., Song, H., Tang, J., 2017. 6.5% Certified Efficiency Sb2Se3 Solar Cells Using PbS Colloidal Quantum Dot Film as Hole-Transporting Layer. ACS Energy Lett. 2 (9), 2125–2132.

Chu, S., Zhao, R., Liu, R., Gao, Y., Wang, X., Liu, C., Chen, J., Zhou, H., 2018. Atomic-layer-deposited ultra-thin VOx film as a hole transport layer for perovskite solar cells. Semicond. Sci. Technol. 33 (11), 115016. https://doi.org/10.1088/1361-6641/aae071.

Crabtree, G.W., Lewis, N.S., 2007. Solar energy conversion. Phys. Today 60 (3), 37–42.

Das, S., Roy, A., Barui, A.K., Alabbasi, M.M.A., Kuncha, M., Sistla, R., Sreedhar, B., Patra, C.R., 2020. Anti-angiogenic vanadium pentoxide nanoparticles for the treatment of melanoma and their in vivo toxicity study. Nanoscale 12 (14), 7604–7621.

El Chaar, L., lamont, L.A., El Zein, N., 2011. Review of photovoltaic technologies. Renew. Sustain. Energy Rev. 15 (5), 2165–2175.

Fang, W., Zhao, J., Wu, T., Huang, Y., Yang, L., Liu, C., Zhang, Q., Huang, K., Yan, Q., 2020. Hydrophilic engineering of VOx-based nanosheets for ambient electrochemical ammonia synthesis at neutral pH. J. Mater. Chem. A 8 (12), 5913–5918.

Green, M., Dunlop, E., Hohl-Ebinger, J., Yoshita, M., Kopidakis, N., Hao, X., 2021. Solar cell efficiency tables (version 57). Prog. Photovoltaics Res. Appl. 29 (1), 3–15.

Green, M.A., Hishikawa, Y., Dunlop, E.D., Levi, D.H., Hohl-Ebinger, J., Ho-Baillie, A.W. Y., 2018. Solar cell efficiency tables (version 51). Prog. Photovoltaics Res. Appl. 26 (1), 3–12.

Guo, L., Zhang, B., Qin, Y., Li, D., Li, L., Qian, X., Yan, F., 2018. Tunable Quasi-One-Dimensional Ribbon Enhanced Light Absorption in Sb_2Se_3 Thin-film Solar Cells Grown by Close-Space Sublimation. Solar RRL 2 (10), 1800128. https://doi.org/10.1002/solr.v2.1010.1002/solr.201800128.

Guo, L., Zhang, B., Ranjit, S., Wall, J., Saurav, S., Hauser, A.J., Xing, G., Li, L., Qian, X., Yan, F., 2019. Interface Engineering via Sputtered Oxygenated CdS: O Window Layer for Highly Efficient Sb2Se3 Thin-Film Solar Cells with Efficiency Above 7%. Solar RRL 3 (10), 1900225. https://doi.org/10.1002/solr.v3.1010.1002/solr.201900225.

Jiang, C., Zhou, J., Tang, R., Lian, W., Wang, X., Lei, X., Zeng, H., Zhu, C., Tang, W., Chen, T., 2021. 9.7%-efficient Sb2(S, Se)3 solar cells with a dithieno[3,2-b: 2′,3′-d] pyrrole-cored hole transporting material. Energy Environ. Sci. 14 (1), 359–364.

Lei, H., Chen, J., Tan, Z., Fang, G., 2019. Review of Recent Progress in Antimony Chalcogenide-Based Solar Cells: Materials and Devices. Solar RRL 3 (6), 1900026. https://doi.org/10.1002/solr.v3.610.1002/solr.201900026.

Leng, M., Luo, M., Chen, C., Qin, S., Chen, J., Zhong, J., Tang, J., 2014. Selenization of Sb2Se3 absorber layer: An efficient step to improve device performance of CdS/Sb2Se3 solar cells. Appl. Phys. Lett. 105 (8), 083905. https://doi.org/10.1063/1.4894170.

Li, D.-B., Yin, X., Grice, C.R., Guan, L., Song, Z., Wang, C., Chen, C., Li, K., Cimaroli, A.J., Awni, R.A., Zhao, D., Song, H., Tang, W., Yan, Y., Tang, J., 2018. Stable and efficient CdS/Sb2Se3 solar cells prepared by scalable close space sublimation. Nano Energy 49, 346–353.

Li, K., Wang, S., Chen, C., Kondrotas, R., Hu, M., Lu, S., Wang, C., Chen, W., Tang, J., 2019a. 7.5% n–i–p Sb2Se3 solar cells with CuSCN as a hole-transport layer. J. Mater. Chem. A 7 (16), 9665–9672.

Li, Z.-Q., Ni, M., Feng, X.-D., 2020. Simulation of the Sb2Se3 solar cell with a hole transport layer. Mater. Res. Express 7 (1), 016416. https://doi.org/10.1088/2053-1591/ab5fa7.

Li, Z., Liang, X., Li, G., Liu, H., Zhang, H., Guo, J., Chen, J., Shen, K., San, X., Yu, W., Schropp, R.E.I., Mai, Y., 2019b. 9.2%-efficient core-shell structured antimony selenide nanorod array solar cells. Nat. Commun. 10 (1), 125.

Li, Z., Liang, X., Li, G., Liu, H., Zhang, H., Guo, J., Chen, J., Shen, K., San, X., Yu, W., Schropp, R.E.I., Mai, Y., 2019c. 9.2%-efficient core-shell structured antimony selenide nanorod array solar cells. Nature. Communications 10 (1), 125.

Manno, D., Serra, A., Di Giulio, M., Micocci, G., Taurino, A., Tepore, A., Berti, D., 1997. Structural and electrical properties of sputtered vanadium oxide thin films for applications as gas sensing material. J. Appl. Phys. 81 (6), 2709–2714.

Mavlonov, A., Razykov, T., Raziq, F., Gan, J., Chantana, J., Kawano, Y.u., Nishimura, T., Wei, H., Zakutayev, A., Minemoto, T., Zu, X., Li, S., Qiao, L., 2020. A review of Sb2Se3 photovoltaic absorber materials and thin-film solar cells. Sol. Energy 201, 227–246.

Nayak, P.K., Mahesh, S., Snaith, H.J., Cahen, D., 2019. Photovoltaic solar cell technologies: analysing the state of the art. Nat. Rev. Mater. 4 (4), 269–285.

Peng, H., Sun, W., Li, Y., Ye, S., Rao, H., Yan, W., Zhou, H., Bian, Z., Huang, C., 2016a. Solution processed inorganic V2O x as interfacial function materials for inverted planar-heterojunction perovskite solar cells with enhanced efficiency. Nano Res. 9 (10), 2960–2971.

Peng, H., Sun, W., Li, Y., Ye, S., Rao, H., Yan, W., Zhou, H., Bian, Z., Huang, C., 2016b. Solution processed inorganic V2Oxas interfacial function materials for inverted planar-heterojunction perovskite solar cells with enhanced efficiency. Nano Res. 9 (10), 2960–2971.

Prześniak-Welenc, M., Łapiński, M., Lewandowski, T., Kościelska, B., Wicikowski, L., Sadowski, W., 2015. The Influence of Thermal Conditions on V_2O_5 Nanostructures Prepared by Sol-Gel Method. Journal of Nanomaterials 2015, 1–8.

Shen, K., Zhang, Y.u., Wang, X., Ou, C., Guo, F., Zhu, H., Liu, C., Gao, Y., Schropp, R.E.I., Li, Z., Liu, X., Mai, Y., 2020. Efficient and Stable Planar n-i-p Sb2Se3 Solar Cells Enabled by Oriented 1D Trigonal Selenium Structures. Adv Sci (Weinh) 7 (16), 2001013. https://doi.org/10.1002/advs.v7.1610.1002/advs.202001013.

Wang, L., Li, D.-B., Li, K., Chen, C., Deng, H.-X., Gao, L., Zhao, Y., Jiang, F., Li, L., Huang, F., He, Y., Song, H., Niu, G., Tang, J., 2017. Stable 6%-efficient Sb2Se3 solar cells with a ZnO buffer layer. Nat. Energy 2 (4). https://doi.org/10.1038/nenergy.2017.46.

Wang, X., Tang, R., Yin, Y., Ju, H., Li, S., Zhu, C., Chen, T., 2019. Interfacial engineering for high efficiency solution processed Sb2Se3 solar cells. Sol. Energy Mater. Sol. Cells 189, 5–10.

Wen, X., Chen, C., Lu, S., Li, K., Kondrotas, R., Zhao, Y., Chen, W., Gao, L., Wang, C., Zhang, J., Niu, G., Tang, J., 2018. Vapor transport deposition of antimony selenide thin film solar cells with 7.6% efficiency. Nature. Communications 9 (1), 2179.

Yang, C., Tartaglino, U., Persson, B.N., 2006. Influence of surface roughness on superhydrophobicity. Phys. Rev. Lett. 97 (11), 116103.

Zakutayev, A., 2017. Brief review of emerging photovoltaic absorbers. Curr. Opin. Green Sustainable Chem. 4, 8–15.

Zeng, K., Xue, D.-J., Tang, J., 2016. Antimony selenide thin-film solar cells. Semicond. Sci. Technol. 31 (6), 063001. https://doi.org/10.1088/0268-1242/31/6/063001.

Zhang, L., Jiang, C., Wu, C., Ju, H., Jiang, G., Liu, W., Zhu, C., Chen, T., 2018. V2O5 as Hole Transporting Material for Efficient All Inorganic Sb2S3 Solar Cells. ACS Appl. Mater. Interfaces 10 (32), 27098–27105.

Zhou, Y., Li, Y., Luo, J., Li, D., Liu, X., Chen, C., Song, H., Ma, J., Xue, D.-J., Yang, B.o., Tang, J., 2017. Buried homojunction in CdS/Sb2Se3 thin film photovoltaics generated by interfacial diffusion. Appl. Phys. Lett. 111 (1), 013901. https://doi.org/10.1063/1.4991539.

Zhou, Y., Wang, L., Chen, S., Qin, S., Liu, X., Chen, J., Xue, D.-J., Luo, M., Cao, Y., Cheng, Y., Sargent, E.H., Tang, J., 2015. Thin-film Sb2Se3 photovoltaics with oriented one-dimensional ribbons and benign grain boundaries. Nat. Photonics 9 (6), 409–415.

Zilberberg, K., Trost, S., Meyer, J., Kahn, A., Behrendt, A., Lützenkirchen-Hecht, D., Frahm, R., Riedl, T., 2011. Inverted Organic Solar Cells with Sol-Gel Processed High Work-Function Vanadium Oxide Hole-Extraction Layers. Adv. Funct. Mater. 21 (24), 4776–4783.